Geophys. J. Int. (2002) **151,** 622–631

Simulated annealing inversion of multimode Rayleigh wave dispersion curves for geological structure

K. S. Beaty, D. R. Schmitt and M. Sacchi

Institute for Geophysical Research, Department of Physics, University of Alberta, Edmonton, Alberta, Canada. E-mail: kbeaty@phys.ualberta.ca

Accepted 2002 June 26. Received 2002 June 6; in original form 2001 October 9

SUMMARY

Simulated annealing was used to invert fundamental and higher-mode Rayleigh wave dispersion curves simultaneously for an *S*-wave velocity profile. The inversion was applied to near-surface seismic data (with a maximum depth of investigation of around 10 m) obtained over a thick lacustrine clay sequence. The geology was described either in terms of discrete layers or by a superposition of Chebyshev polynomials in the inversion and the contrasting results compared. Simulated annealing allows for considerable flexibility in model definition and parametrization and seeks a global rather than a local minimum in a misfit function. It has the added advantage in that it can be used to determine uncertainties in inversion parameters, thereby highlighting features in an inverted profile that should be interpreted with caution. Results show that simulated annealing works well for the inversion of multimodal near-surface Rayleigh wave dispersion curves relative to the same inversion that employs only the fundamental mode.

Key words: near-surface geophysics, Rayleigh wave dispersion, simulated annealing.

1 INTRODUCTION

Rayleigh waves travel along the earth–air interface and are a result of combined *P* waves and vertically polarized *S* waves interacting with the free surface boundary. Rayleigh waves are dispersive over layered geologies, a property that can be exploited in geophysical investigations. Shorter wavelengths are sensitive to the velocities of the near-surface materials, while longer wavelengths probe the deeper subsurface. Generally, the Rayleigh wave peak sensitivity is to a depth of between one-third and one-half of a wavelength and are most sensitive to shear wave velocity but also depend weakly on the *P*-wave and density profiles.

Earthquake seismologists have long made use of surface waves, especially Rayleigh waves, to investigate the *P*- and *S*-wave velocity structure of the crust and upper mantle (Lay & Wallace 1995). Surface wave dispersion, however, works equally well at smaller scales and has become an important tool for probing the shallow subsurface in environmental (Miller *et al.* 1999a,b,c; Long *et al.* 1999) and geotechnical engineering applications (Stokoe & Nazarian 1985; Nazarian & Stokoe 1986).

A dispersion curve shows the velocity of the wave at each wavelength or frequency. In layered structures, Rayleigh wave dispersion curves are, in general, multimodal. However, most studies assume the surface wave packet to be composed of a fundamental only, despite the fact that higher Rayleigh modes often contain significant energy. Higher modes provide information to greater depths than the fundamental mode and improving the accuracy of an inverted *S*-wave velocity profile (Xia *et al.* 2000). Once reliable dispersion curves have been obtained, they must be inverted to determine the shear wave velocity profile with depth (Xia *et al.* 1999; Nazarian & Stokoe 1986). However, the Rayleigh wave velocities are related to the velocity structure in a complex way, making the inversion of such curves problematic.

Simulated annealing is a directed Monte Carlo inversion method that is well suited to finding the global minimum of a non-linear error function. Simulated annealing has recently been used to invert Rayleigh wave dispersion data for crustal and upper-mantle shear wave velocity profile using only the fundamental mode (Martinez *et al.* 2000). However, in near-surface investigations higher-order Rayleigh wave modes often contain sizeable fractions of the overall wave energy. Incorporation of the dispersion of higher modes improves the accuracy of the inversion process (Tokimatsu *et al.* 1992; Xia *et al.* 2000) and for this reason are included in the present analysis. In this paper, the non-linear simulated annealing technique is tested on a known synthetic set of dispersion curves and then applied to multimodal dispersion curves observed in a near-surface survey. A variety of polynomial and discrete layer representations of the geological structure are employed in the inversion. Finally, an uncertainty analysis is carried out to highlight the sections of the inversion where the most care must be taken in interpretation.

2 FORWARD MODELLING AND INVERSE THEORY

With surface wave studies, as with most other geophysical surveys, the main objective is to gain an understanding of the physical characteristics of the earth materials present at the study site. Rayleigh

wave dispersion in an elastic medium is dependent on density, the *P*- and the *S*-wave velocities. The strongest dependence is on the *S*-wave velocity (Ewing *et al.* 1957; Fowler 1990). This section will first describe the forward modelling technique used to obtain theoretical dispersion curves in an elastic, layered medium and then proceed to outline the inversion technique used to obtain velocity profiles and uncertainties in the velocities from the measured dispersion curves.

2.1 Rayleigh waves in a layered medium

Rayleigh waves are characterized by retrograde elliptical particle motion at the surface. The amplitude of the wave decays exponentially with depth (Ewing *et al.* 1957). Only a very few simple cases, such as the homogeneous half-space and a single layer overlying a half-space, have analytic solutions that are easily obtained. In reality, however, geological structure is rarely that simple and numerical methods for determining Rayleigh wave dispersion curves for more complex geological models must be explored. Matrix methods are often used to determine the eigenvalues and eigenfunctions for the case of a vertically varying medium consisting of a set of n homogeneous isotropic layers overlying a homogeneous half-space (Fig. 1). For a layered media, Rayleigh waves arise from the interference of P and SV waves (vertically polarized shear waves) with the free surface.

Thomson (1950) developed the original matrix method for solving this boundary value problem, later corrected by Haskell (1953). Subsequent researchers reformulated the problem using global matrices in such a way that numerical stability was improved and solutions could be obtained for much higher frequencies than previously possible (Knopoff 1964; Schwab & Knopoff 1972). Reduced δ-matrix formulations have also been derived (Watson 1970), but can be shown to be identical to Knopoff's method (Schwab 1970).

Abo-Zena (1979) developed further improvements over the method described in Schwab & Knopoff (1972) in terms of the ability of the method to handle high frequencies. Menke (1979) noticed that the method of Abo-Zena (1979) could be simplified by computing only the independent matrix elements, resulting in improvements in both speed and accuracy.

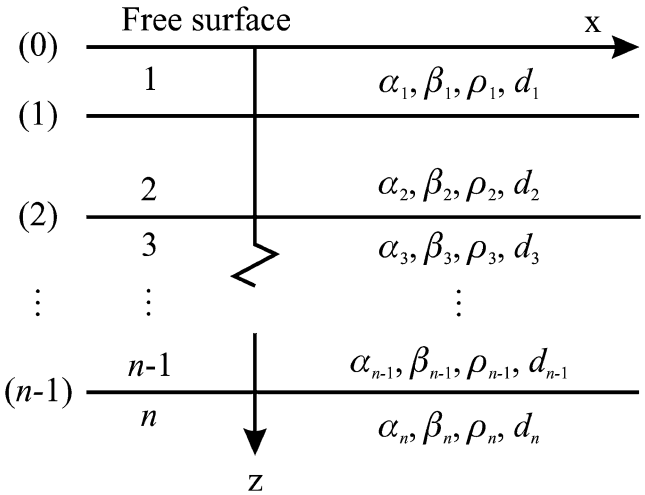

Figure 1. Diagram showing layered structure with n layers. Layers and interfaces are numbered. Each layer has P- and S-wave velocities (α and β), and density (ρ) and thickness (d).

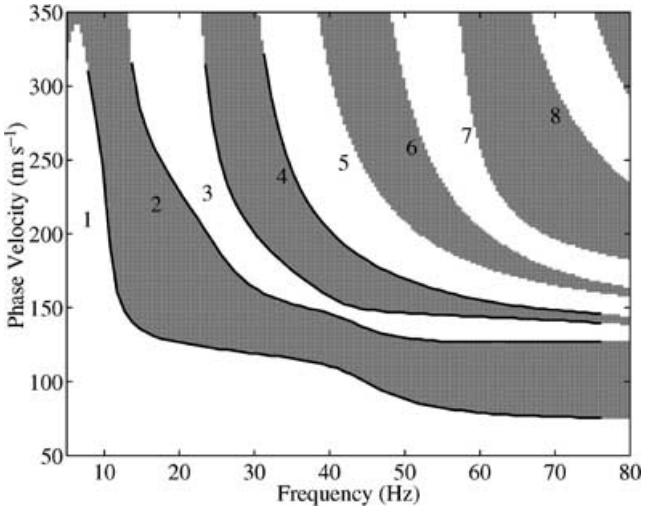

Figure 2. White and grey bands represent positive and negative values of the dispersion function, respectively, with roots representing the various modes at the change in shade. The solid lines represent the first four roots (zeros) of the dispersion function. The numbers on the image to the left of each mode indicate the mode order.

A wide variety of other techniques have been used to calculate Rayleigh wave dispersion curves in layered media. Numerical methods such as the Runge–Kutta or the Rayleigh–Ritz variational procedure have been used (Takeuchi & Saito 1972; Wiggins 1976). The methods thus far have all been developed for global seismology applications but they scale to any size problem. One other method, similar to the propagator matrix methods mentioned above, has been employed in some geotechnical studies (Ganji *et al.* 1998). The stiffness matrix method approaches the problem from the perspective of dynamic loading of the soils and their response to the load (Wolf 1985; Kausel & Roesset 1981; Kausel & Peek 1982).

Menke's version was chosen for forward modelling for this study because matrix propagator methods are relatively easy to implement, are well studied and because in simulated annealing inversion choosing a linear model is not a necessity. The model yields a dispersion function $D(\omega, c)$, the roots of which correspond to Rayleigh wave dispersion curves. The bisection method, a standard root-finding algorithm, was used to delineate the dispersion curves for each mode (Press *et al.* 1997). An example showing the dispersion function and the first four dispersion curve modes is displayed in Fig. 2. The parameters used in this calculation can be found in Table 1.

2.2 The inversion of Rayleigh wave dispersion curves

Simulated annealing, a directed Monte Carlo method (Kirkpatrick *et al.* 1983; Chunduru *et al.* 1996), was here used to perform the inversion of the Rayleigh wave dispersion curves for the velocity structure. Simulated annealing, like other geophysical inversion

Table 1. Parameters used in calculating the dispersion curves shown in Fig. 2 where d is the thickness of the layer, α is the P-wave velocity β is the S-wave velocity and ρ is the density.

Layer	d (m)	α (m s^{-1})	β (m s^{-1})	ρ (g cm^{-3})
1	0.8	185	80	1.18
2	3.7	480	140	1.78
3	2.5	1650	140	1.78
4	∞	1650	1040	2.18

procedures, seeks to minimize a misfit function $E(\mathbf{m})$, where $\mathbf{m}$ is the model vector, which in our particular case involves the *P*- and *S*-wave velocity–depth profiles and the density–depth profile. The advantage of this technique is that it is not limited to linear problems and seeks the global rather than a local minimum in the misfit function. The definitions of the error function and the forward model are independent of the inversion algorithm so there is freedom to define both in whatever way best suits the problem. Furthermore, the method allows for some estimates of uncertainty to be obtained. The disadvantage of simulated annealing is that it can be more expensive computationally than linearized methods.

Simulated annealing has only recently been used to find crustal and upper-mantle velocity profiles by inverting fundamental mode dispersion curves (Martinez *et al.* 2000). Most researchers have employed linearized methods (Ganji *et al.* 1998; Aki & Richards 1980) or else a combination of linear and non-linear methods (Xia *et al.* 1999). Roth & Holliger (1999), however, used a genetic algorithm, which is another example of a directed Monte Carlo inversion technique. They obtained both *P*- and *S*-wave velocity profiles by inverting both fundamental mode Rayleigh and guided-wave dispersion curves. Simulated annealing will be applied to fundamental and higher-order Rayleigh wave dispersion curves in this study and guided waves will not be examined.

To understand the concept of simulated annealing, an analogy can be drawn between the model parameters of an optimization problem and particles in a physical system. Physical annealing occurs when a solid is heated up until all the particles are randomly distributed in the liquid phase. If the material is cooled slowly then it will form a crystalline solid, whereas if it is cooled too quickly it will freeze into an amorphous glass (a local rather than a global minimum in energy). The probability at each temperature T that the system will be in state i with energy E_i is

$$P(E_i) = \frac{\exp(-E_i/k_{\mathrm{B}}T)}{\sum_{j\in S}\exp(-E_j/k_{\mathrm{B}}T)}, \tag{1}$$

where S contains all possible particle configurations and k_{B} is Boltzmann's constant. For geophysical inversions, k_{B} is set to 1 and instead of energy the probability distribution function becomes a function of possible sets of model parameters $\mathbf{m}_i$. The 'temperature' T takes on the dimensions of the error and can be looked upon as a control parameter (Sen & Stoffa 1995; Ingber 1989). By semi-randomly accepting some models that actually increase the error, the algorithm attempts to avoid becoming trapped in local minima. At low temperatures this reduces to a greedy algorithm, meaning that it only accepts models that decrease the error function. Convergence is achieved when the error or energy remains the same for several iterations.

The Metropolis algorithm (Metropolis *et al.* 1953) is perhaps the best known simulated annealing method. An outline of the basic algorithm (Fig. 3) is provided in Sen & Stoffa (1995). An initial model $\mathbf{m}_0$ is selected and the corresponding misfit $E(\mathbf{m}_0)$ is determined. A new model is drawn at random from a uniform distribution and the misfit is found for the new model. If the misfit has improved then the new model is always accepted. If the misfit has become larger then the new model is accepted with the temperature-dependent probability $P = \exp(-\Delta E/T)$. This process is repeated as the temperature is gradually decreased until the misfit remains the same for a number of iterations. The necessary and sufficient condition for convergence to the global minimum is given by the cooling schedule

$$T(i) = \frac{T_0}{\ln i}, \tag{2}$$

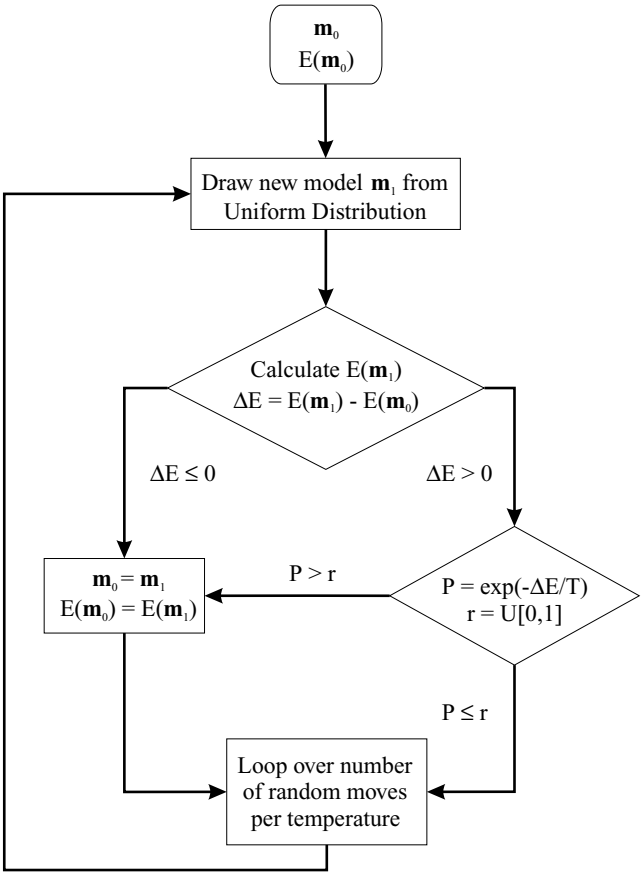

Figure 3. Flow chart of the operations carried out at each temperature for the Metropolis simulated annealing algorithm.

where i is the iteration number and T_0 is a sufficiently high initial temperature (Geman & Geman 1984).

Fast simulated annealing (FSA), a variant of the Metropolis algorithm, was proposed by Szu & Hartley (1987). This algorithm is identical to the Metropolis algorithm with the exception that model parameters are drawn from a Cauchy-like distribution instead of a uniform distribution. A Cauchy-like distribution is given by

$$P(\Delta\mathbf{m}) \propto \frac{T}{\sqrt{\Delta\mathbf{m}^2 + T^2}}. \tag{3}$$

At high temperature the distribution approaches uniformity while at lower temperatures it favours smaller perturbations (Fig. 4). For FSA the cooling schedule should not exceed

$$T(i) = \frac{T_0}{i}, \tag{4}$$

which is much faster than for conventional simulated annealing.

The forward model for Rayleigh wave dispersion being used here (see above) represents the earth in terms of a discrete set of layers overlying a homogeneous half-space. Each layer has its own density, *P*-wave velocity and *S*-wave velocity. Density and *P*-wave velocity both have very little impact on the dispersion curves and are taken as a fixed parameters on the basis of additional knowledge. This still leaves n parameters that need to be inverted for, where n is the number of layers.

In contrast, if a smooth velocity profile is expected then $\alpha(z)$ and $\beta(z)$ can be alternatively represented using a sum of Chebyshev polynomials (Arfken & Weber 1995; Grechka *et al.* 1996). The inverse problem can then be structured to solve for the coefficients of

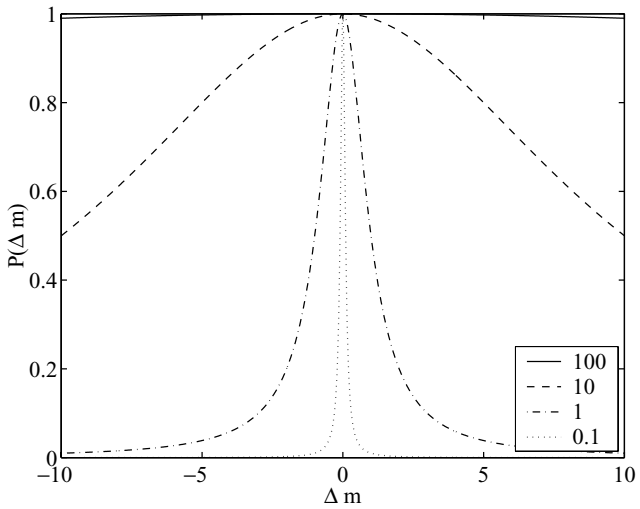

Figure 4. Diagram showing the shape of a Cauchy-like probability distribution for temperatures of 0.1, 1, 10 and 100.

this series instead of the velocities for each layer. Now instead of inverting for a large number of velocity parameters to approximate a continuous medium, $\beta(z)$ can be represented by only four or five coefficients. The forward model used in this study requires a set of discrete layers, so when evaluating the misfit function the polynomial representation of the velocity profile must be discretized. To achieve this discretization, the velocity of a given layer z is taken as the value of the polynomial series at the centre of that layer. At each step of the inversion the polynomial coefficients are varied, the velocity profile is discretized and the misfit evaluated. A particular set of polynomial coefficients is accepted or rejected based on the temperature and the misfit value in the same manner as for the discrete case.

2.3 Initial model and misfit function

A reasonable initial model can be determined using bulk density measurements gathered from soil coring and velocities determined from the vertical seismic profile. According to the results of Xia *et al.* (1999, 2000), a 25 per cent error in both the *P*-wave velocity profile and the density profile will result in an error of only 7 per cent in the *S*-wave velocity profile. As such, good estimates of *P*-wave velocity and density values that are then held constant should be sufficient to obtain a reasonable *S*-wave velocity profile.

The inverse procedure will set out to find the global minimum of the objective function. For each mode the objective function is defined as

$$E = \frac{1}{N}\sum_{f}\left(d^{f}_{\text{obs}} - d^{f}_{\text{pred}}\right)^{2}, \tag{5}$$

where d^{f}_{obs} is the phase velocity value at frequency f determined from the observed data, d^{f}_{pred} is the phase velocity predicted by the forward model at frequency f and the sum is over all N frequencies. Any mode can be inverted for separately, or the overall misfit function can be represented by a weighted sum of objective functions from all modes present in the data.

For multimode inversions, the weighted sum of the error functions for each mode was used, eq. (5). The fundamental mode was arbitrarily assigned a weight of 0.5 and the two higher modes were assigned weights of 0.25 each. The rationale behind this choice was that the fundamental mode contained more energy and was easier to pick out than the two higher modes. With real dispersion curves there is some ambiguity as to the veracity of assigning the second and third modes. For example, it is possible that the curves that have been labelled as the second and third modes might actually be the third and fourth. To account for this ambiguity the two higher modes were compared with the second and third ones, and the third and fourth calculated modes at each iteration and the minimum misfit between these two cases were accepted.

For a good choice of initial temperature, the ratio of accepted models to rejected models after a large number of iterations at a constant temperature should be greater than 50 per cent but less than 100 per cent. If the ratio is less than 50 per cent then the temperature may not be high enough to escape local minima and if the initial temperature is too high then it will take a much larger number of iterations than necessary for the algorithm to converge.

2.4 Uncertainty estimation

Metropolis simulated annealing has properties that make it suitable for estimating the uncertainty in the results of an inversion (Sen & Stoffa 1995). After a large number of iterations at a constant temperature an equilibrium distribution will be attained independent of the starting model given by the Gibbs probability density function

$$p_{\text{Gibbs}}(\mathbf{m}) = \frac{\exp\left[-E(\mathbf{m})/T\right]}{\sum_{\mathbf{m}}\exp\left[-E(\mathbf{m})/T\right]}, \tag{6}$$

where $E(\mathbf{m})$ is the value of the error function for the model $\mathbf{m}$ and the temperature T controls the width of the distribution. The sum in the denominator is taken over all models.

An expression for the uncertainty in the inversion results can be developed using Bayesian statistics (Sen & Stoffa 1995). If the errors in the theory and the data are assumed to be Gaussian, then the posterior probability density $\sigma(\mathbf{m}\,|\,\mathbf{d}_{\text{obs}})$ of model $\mathbf{m}$ given the observed data $\mathbf{d}_{\text{obs}}$ can be expressed as

$$\sigma(\mathbf{m}\,|\,\mathbf{d}_{\text{obs}}) \propto \exp[-E(\mathbf{m})]p_{\text{prior}}(\mathbf{m}), \tag{7}$$

where $p_{\text{prior}}(\mathbf{m})$ is the prior probability distribution for the model independent of the data. Note that in this equation, $E(\mathbf{m})$ is meant to have been normalized by the data uncertainty. Comparison of this expression with eq. (6) shows that eq. (7) is essentially the Gibbs probability density function at temperature $T = 1$ if the prior distribution is uniform. Alternately, if the uncertainty in the data is not well known, the final temperature can be used as an estimate and Metropolis simulated annealing run for many iterations at $T = T_f$ should provide a good estimate of the model uncertainty (Martinez *et al.* 2000). For this study an estimate of uncertainty is available (Fig. 5d) so a temperature of $T = \bar{\sigma}^2 = 5.04\ \text{m}^2\ \text{s}^{-2}$, based on the square of the average uncertainty in the measured phase velocities, was used.

Metropolis simulated annealing, when it is run for a large number of iterations, is also referred to as a Gibbs sampler. If it is run at a temperature T of T_f it may be used as a Monte Carlo importance sampling technique to evaluate quantities such as the marginal posterior probability density function, mean and covariance. The marginal posterior probability density function can be found directly from the frequency distribution of the model parameters. The mean can be approximated by the following equation:

$$\langle\mathbf{m}\rangle \cong \frac{1}{NM}\sum_{j=1}^{NM}\mathbf{m}_{j}, \tag{8}$$

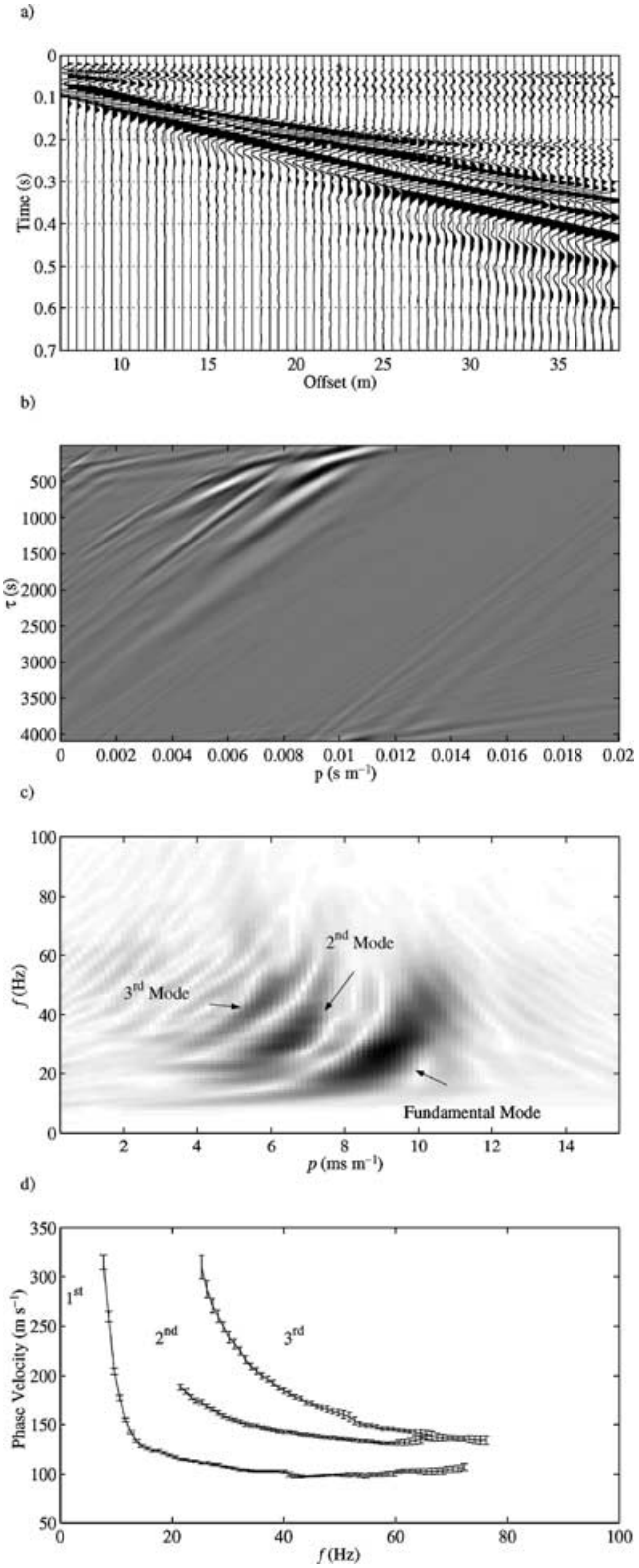

Figure 5. (a) Stacked traces recorded on 1999 September 9 (normalized). (b) τ–p transform of the traces, (c) f–p map of the data and (d) Rayleigh wave dispersion curves for three modes obtained from the f–p map shown in (c).

where $\mathbf{m}_1, \mathbf{m}_2, \ldots, \mathbf{m}_{NM}$ are column vectors of model parameters chosen by the Gibbs sampler and NM is the total number of models used. The covariance will be given by

$$\boldsymbol{C}_M \cong \frac{1}{NM} \sum_{j=1}^{NM} (\mathbf{m}_j - \langle \mathbf{m} \rangle)\,(\mathbf{m}_j - \langle \mathbf{m} \rangle)^{\mathrm{T}}. \tag{9}$$

The standard deviations in the individual model parameters are given by the square root of the diagonal elements of the posterior covariance matrix. The mean and standard deviation values for the model parameters will give an estimate of the uncertainty in the inverted profile (Sen & Stoffa 1995).

Even though a large number of iterations is necessary to obtain a well-defined posterior probability density function, our tests show that several thousand iterations may give a reasonable estimate of the means and standard deviations of model parameters. Uncertainty estimates drawn from a low number of iterations should be interpreted with caution (Beaty 2000).

3 INVERSION RESULTS

The inversion method described above was tested on a data set obtained at the Edmonton Research Station in Edmonton, Alberta, Canada on 1999 September 9. The geology of the study site, as determined though the soil coring, is shown in Table 2. Ground-penetrating radar profiles were acquired to verify the lateral uniformity of the site, an assumption that was made in the forward modelling. The site characterization is described in detail in Beaty (2000).

One series of raw, vertical component, seismic traces from Beaty and Schmitt (in prep.) along with windowed Rayleigh waves are shown in Fig. 5. Dispersion curves (Fig. 5d) were obtained from Rayleigh wave data using a method involving first a Radon or intercept–slowness (τ–p) transform (Fig. 5b) followed by a 1-D Fourier transform along the τ direction (McMechan & Yedlin 1981). The frequency–slowness or f–p map (Fig. 5c) shows three high-amplitude regions corresponding to three Rayleigh wave modes. Dispersion curves (Fig. 5d) for each mode are then derived by choosing the peaks of the high-amplitude regions and taking the inverse of the slowness to obtain the phase velocity. The error in the dispersion picks is estimated using a bootstrapping technique (Efron & Tibishirani 1993).

Inversions were carried out first on a set of synthetic dispersion curves (Fig. 6) using a simple layered profile that was based loosely on the velocity and density information for the Edmonton Research Station obtained from the vertical seismic profile (VSP) profile and soil core measurements (see below). The object of this inversion of synthetic dispersion curves was to determine the accuracy with which the shear wave profile could be determined with depth and to test out the discretization scheme. This resolution information can later be related to the expected resolution of the inversion profiles from the observed dispersion curves.

Inversions on the real data were carried out using several different means of parametrizing the shear wave velocity model. Sums of either five or seven Chebyshev polynomials represented the velocity model as a smooth profile in the first test and a series of discrete layers was used in the second test. Sources of error in the inversion

Table 2. Geology of the study site as determined from core samples.

Depth Range	Thickness	Geology
0–0.3 m	0.3 m	Black top soil
0.3–1.5 m	1.2 m	Grey, brown clay-like soil
1.5–6.7 m	5.2 m	Lacustrine deposits
6.7–8.5 m	1.8 m	Wet, sandy and silty clay
8.5–10+ m	1.5+ m	Compacted glacial tills

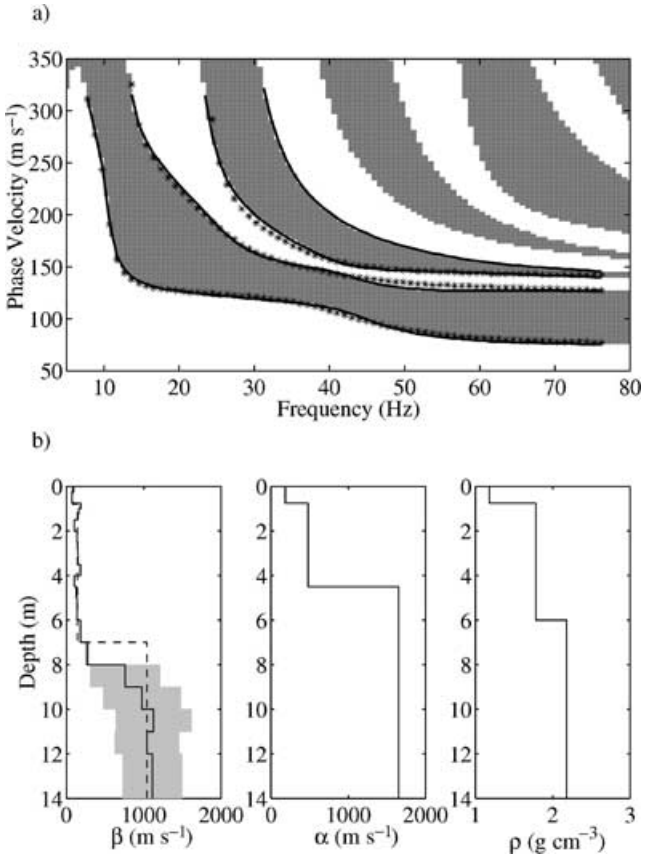

Figure 6. (a) Inversion results using 21 independent layers to represent the theoretical shear wave velocity profile. White and grey bands represent positive and negative values of the dispersion function, respectively. The solid lines represent the roots (zeros) of the dispersion function. The data used in the inversion are plotted as asterisks. These are test data generated using the parameters in Table 1. (b) The shear wave velocity profile (solid line) shown in the left-hand panel is the result of an inversion where 21 independent layers were used to represent the profile. The shaded area represents the velocity range within one standard deviation from the mean. The dashed line delineates the shear wave profile used to generate the synthetic data. The *P*-wave (middle) and density (right) profiles were held constant.

results include inaccuracies in receiver placement, in the *P*-wave and density profiles assumed for the inversion, and in the assumption that the geology is a set of homogeneous and isotropic layers.

Geotechnical engineering studies typically use 60–70 dispersion points from a single mode to invert for 10–15 layers. The number of points available for the fundamental mode dispersion curve falls within this range but the total number of points used in the present inversions is greater (167) as the additional phase velocities from the second and third modes are also employed.

A maximum depth of resolution for a Rayleigh wave dispersion survey is typically estimated as 0.5 to 1 λ_{max} (Rix & Leipski 1991). The September 9 data have a maximum wavelength of 40 m near 10 Hz. Preliminary results here show instability in resolving depths greater than ∼12 m and this was chosen as the top of the infinite half-space for this study. Clearly, there are limitations to this simple generalization but it is a useful first approximation.

Conversely, the minimum thickness that can be resolved immediately at the surface is expected to be half of the minimum wavelength recorded (Stokoe *et al.* 1994). This corresponds to a layer thickness of ∼0.7 m for this survey. Thinner layers, however, will be used in the discretization of the profile because these rules of thumb were developed for surveys where only one mode was considered, whereas in this study all three modes will be used in the inversions. The discretization of the model parameters was chosen as follows: thicknesses of 0.25 m down to 1.5 m, then 0.5 m thicknesses down to 5 m and 1 m down to 12 m for a total of 21 layers. This last layer is taken as an infinite half-space extending downwards from 12 m. This discretization scheme was adopted for the inversion of the synthetic and the experimental data.

3.1 Synthetic test example

Inversions were carried out first on a simple test profile with a velocity and density structure (Fig. 6) similar to that of the Edmonton Research Station site as determined by the vertical borehole seismic profile (Beaty & Schmitt, in prep.) and the soil bulk density measurements. Hypothetical dispersion curves (Fig. 6) were calculated from the profiles and the inversion was carried out by inverting for the shear wave velocities for each of the 21 layers used in the discretization scheme. No noise was added to the hypothetical curves.

The theoretical dispersion curves found through the inversion match very closely, but not exactly, with the synthetic dispersion curves (Fig. 6). Certainly the theoretical curves are within the experimental error of the observed data at the Edmonton Research Station. The dispersion curves are calculated to a specified tolerance that has been set to ± 1 m s^{-1}, also within the experimental error of the surveys. The velocity profile found through inversion, however, does not match very well with the true profile below a depth of ∼7 m (Fig. 6). Uncertainty analysis, carried out using 2480 iterations of Metropolis SA at $T = 1$ (assumes the average σ of the data is around 1 m s^{-1}), reveals that the velocities of layers at 8 m and below can only be resolved very coarsely. Standard deviations in this region are of the order of 400–500 m s^{-1}. The discrepancy between the velocity of the layer between 7 and 8 m found through inversion and that of the true profile is outside of the error region found through the uncertainty analysis. This is an indication that at a depth of 7 m given a similar velocity profile, the depth to a transition can be resolved only to ± 1 m.

Agreement of the inverted parameters to the true profile is much better in the first 7 m. There are small fluctuations that are approximately 8 or 9 m s^{-1} (10–11 per cent) from the true *S*-wave velocity in the topmost layer and from 1 to 53 m s^{-1} (1–38 per cent) in the region from 0.75 to 7 m. The uncertainty analysis in this region has underestimated the error in most of these velocities in this region, a phenomenon that could be related to the small number of iterations used in the importance sampling. The uncertainty in depth, the lower resolution of the deeper layers, and the level of underestimation in the uncertainty of the upper layers should all be taken into consideration when interpreting the inversion profiles from the real data.

3.2 Inversion of experimental data

Inversions were carried out on the data obtained on 1999 September 9. The starting model was chosen by fitting Chebyshev polynomials to the *P*- and *S*-wave velocity profiles determined from the VSP survey and to the bulk density measurements made on the soil cores (Beaty 2000). The theoretical dispersion curves generated using these data provide a marginal fit to the fundamental mode (not shown) but the phase velocities are too low in general and the shape of the curve is not the same in the low-frequency region. The fit of the model to the second and third modes is much worse. The

second and third mode data tend towards the theoretical second and third modes at low frequencies and towards the third and fourth modes at higher frequencies. The layers were discretized according to the 21-layer scheme mentioned earlier. Choosing an initial model that is close to the best-fitting solution is much more important for other inversion methods than for simulated annealing but starting close to the solution may allow the simulated annealing inversion to converge more quickly.

In the first attempt, five Chebyshev coefficients represented the shear wave velocity profile. A very good match between the observed data and the theoretical dispersion curves is obtained (Fig. 7). Small discrepancies exist in the region between 30 and 60 Hz for the fundamental mode and at the low-frequency end of the third mode (below 35 Hz). The reason for this latter discrepancy will be revisited later in this discussion.

The shear wave velocity profile found through this inversion is displayed in Fig. 7 along with the *P*-wave velocity and density profiles that were held constant. The resultant *S*-wave velocity profile shows slightly higher velocities at the surface followed by a slight decrease and then a gradual increase in velocity to a maximum of $\sim$650 m s^{-1}.

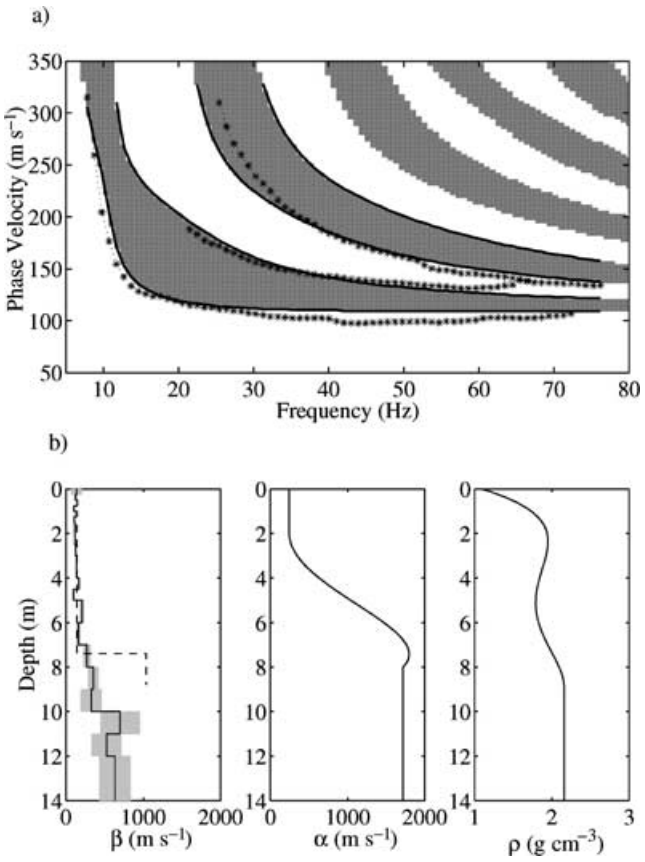

Figure 7. Results of inversion on observed dispersion curves. (a) Inversion results using five Chebyshev polynomials to represent the shear wave velocity profile. White and grey bands represent positive and negative values, respectively. The solid lines represent the roots of the dispersion function to be compared against the observed dispersive velocities from Fig. 5 plotted as asterisks. (b) The shear wave velocity profile shown in the left-hand panel is the result of an inversion where five Chebyshev polynomials were used to represent the profile (solid line). The shaded area shows one standard deviation about the mean (solid line) found through importance sampling. The dashed line is the *S*-wave profile obtained from the VSP survey. The *P*-wave (middle) and density (right) profiles were held constant. Both are plotted as smooth Chebyshev profiles. In practice these profiles are discretized in the same manner as the *S*-wave profile—the polynomial representation is evaluated at the centre of each of the layers and that value is used to represent the parameter value for that layer.

Uncertainty runs on the Chebyshev profile yielded almost no variation in the polynomial coefficients and was thus not a good estimator of uncertainty in the *S*-wave velocity profile. Instead, the Chebyshev profiles obtained through inversion were discretized. The uncertainty analysis was carried out on the discretized profiles to gather information on the mean and standard deviation of the *S*-wave velocities of each layer rather than the Chebyshev parameters.

The uncertainty analysis shows that the upper part of the profile has little uncertainty associated with it, except for the topmost layer. The mean values and higher standard deviations in the section from 7 to 10 m suggest that a faster transition occurs with depth to higher velocities than allowed by the polynomial parametrization in agreement with the known transition from clay to compacted till. Below 10 m the uncertainty increases drastically, indicating a lack of sensitivity of the data for these deeper layers. The sensitivity to deeper layers could be improved by placing more weight on the misfit of the lower-frequency information but the most reliable way to deal with this problem in practice would be to use detectors capable of detecting lower frequencies. The geophones used in this survey provide adequate sensitivity only down to $\sim$10 Hz.

A similar inversion was attempted using seven Chebyshev coefficients to represent the *S*-wave velocity profile. For this inversion an additional parameter, the *P*- to *S*-wave velocity ratio, α/β, was allowed to vary in order to allow variations in the *P*-wave velocity profile without the addition of too many parameters. The use of additional polynomials in the inversion makes it possible to image more rapid geological variations. The misfit curve for this inversion is shown in Fig. 8. The match between the observed and theoretical dispersion curves (Fig. 8) is better than in the five-polynomial case at the low-frequency end, especially for the third mode. At the high-frequency end, however, it is slightly worse for the fundamental and second modes. This may indicate that representation of the *P*-wave velocity profile by a single factor coupling it to the *S*-wave velocities may not be a good representation. The uncertainty estimates show that the resolution down to $\sim$5 m is very good and then it abruptly deteriorates. The uncertainty in the *P*-wave profile shows that only a very narrow range of *P*- to *S*-wave velocity ratios will fit the data well for the inverted *S*-wave velocity profile. The value of the α/β parameter was found to be 1.68 ± 0.03.

The inversion of the September 9 data set was also carried out by inverting directly for the shear wave velocities for 21 layers. The match of the theoretical curve to the observed dispersion curve (Fig. 9) is better than for either of the Chebyshev polynomial inversions. This shear wave velocity profile does not show the increased velocity in the topmost layer as the Chebyshev profiles suggested (Figs 7 and 8). The profile is almost constant down to 4.5 m when there is a slight increase in velocity followed by a much larger jump at 8 m. The uncertainties in the velocities down to 7 m are quite small ($<$25 m s^{-1}). Note that in the top layer the velocity uncertainty is higher ($\pm$57 m s^{-1}). Below 7 m uncertainties increase substantially, suggesting that care should be taken in interpreting *S*-wave velocities in this region.

Manipulation of the *S*-wave velocity profile showed that if the velocity was increased in the layer between 7 and 8 m then the match between the theoretical and observed dispersion curves for the third mode deteriorates at frequencies below 35 Hz relative to the five Chebyshev coefficients case. This suggests that there is a sharper increase in velocity at this point than the polynomials are capable

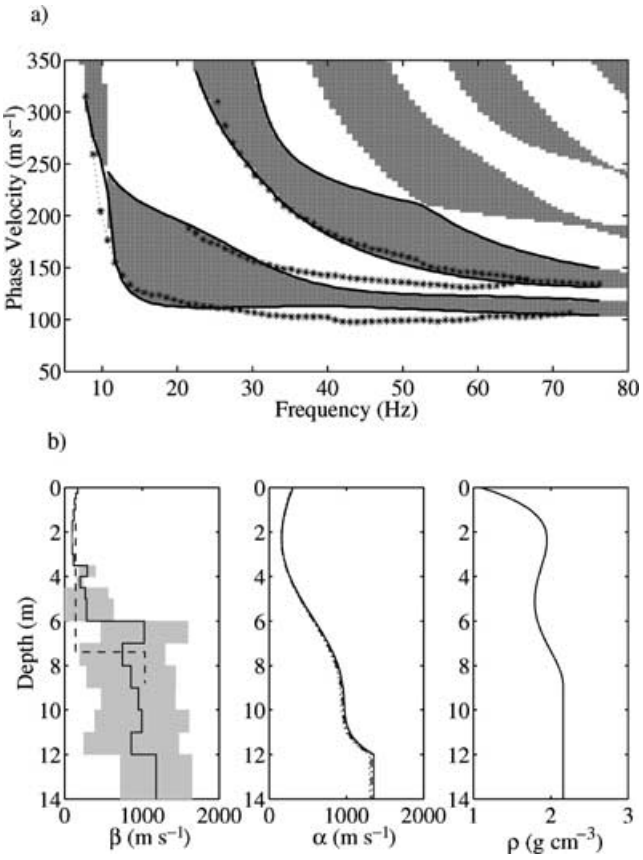

Figure 8. (a) Inversion results using seven Chebyshev polynomials to represent the shear wave velocity profile and a multiplicative factor to represent the *P*-wave profile. White and grey bands represent positive and negative values, respectively. The solid lines represent the roots of the dispersion function and the data are plotted as asterisks. (b) The shear wave velocity profile shown in the left-hand panel is the result of an inversion where seven Chebyshev polynomials were used to represent the profile. The shaded region represents the range found through the importance sampling technique. The dashed line is the *S*-wave profile obtained from the VSP survey. The *P*-wave profile (middle) was calculated by multiplying the shear wave velocity profile by a constant and the density profile (right) was held constant.

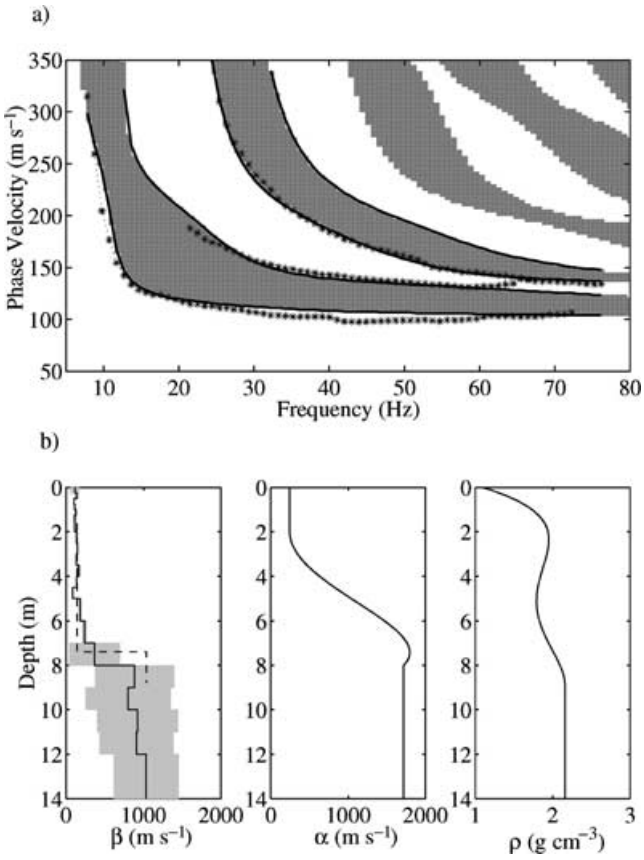

Figure 9. (a) Inversion results using 21 independent layers to represent the shear wave velocity profile. White and grey bands represent positive and negative values, respectively. The solid lines represent the roots of the dispersion function and the data are plotted as asterisks. (b) The shear wave velocity profile shown in the left-hand panel is the result of an inversion where 21 independent layers were used to represent the profile. The shaded area shows one standard deviation about the mean (solid line) found through importance sampling. The dashed line is the *S*-wave profile obtained from the VSP survey. The *P*-wave (middle) and density (right) profiles were held constant.

of representing. The velocity profile shown in Fig. 9 is probably the closest to the true profile but the exact value of the *S*-wave velocity below 8 m has a large error associated with it. The error in the depth to the top of this higher-velocity layer could be as much as ± 1 m, as indicated by the synthetic example.

This profile corresponds well with the geological profile determined from soil core analysis (Table 2). The thin layer of top soil (0.3 m thick) is probably too thin to be resolved. The velocity profile down to $\sim$4.5 m is close to a constant velocity. This region contains soils mixed with clay followed by pure clay. The slightly higher velocities from 4.5 to 7 m might be because of the increasing pressure on the clays or the presence of water, but the change is very small and may not be significant. Between 7 and 8 m there is again a slight increase in velocity where the layer of wet sand was found in the soil core. Below 8 m (± 1 m) there is strong evidence for a sharp velocity change corresponding to the top of the glacial tills, which is at a depth of 8.5 m according to an analysis of the soil core samples.

All of the inversions presented thus far have employed all three modes. For comparison, the 21-layer inversion procedure was rerun based on the fundamental mode data only. The results (Fig. 10) show excellent agreement between the fundamental mode theoretical dispersion curve and the data, but it is clear that the result shown does not match either of the higher-order modes and the *S*-wave velocity–depth profile does not match the geology or the VSP results and the three-mode inversion (Fig. 9). An uncertainty analysis was not performed on these inversion results.

4 CONCLUSIONS

In this study, simulated annealing has been used to invert multimode Rayleigh wave dispersion data for *S*-wave velocity–depth profiles. The incorporation of multiple modes into the inversion process offers significant improvement over inversions using only fundamental modes in near-surface studies where significant energy is carried by the higher modes. Profiles found using multiple modes are better resolved, have smaller uncertainties and are much more reliable.

Inversion of the three Rayleigh mode dispersion curves using a fast simulated annealing algorithm (Sen & Stoffa 1995) coupled with a matrix propagator forward modelling technique (Menke 1979) yields *S*-wave velocity profiles that agree well with geological

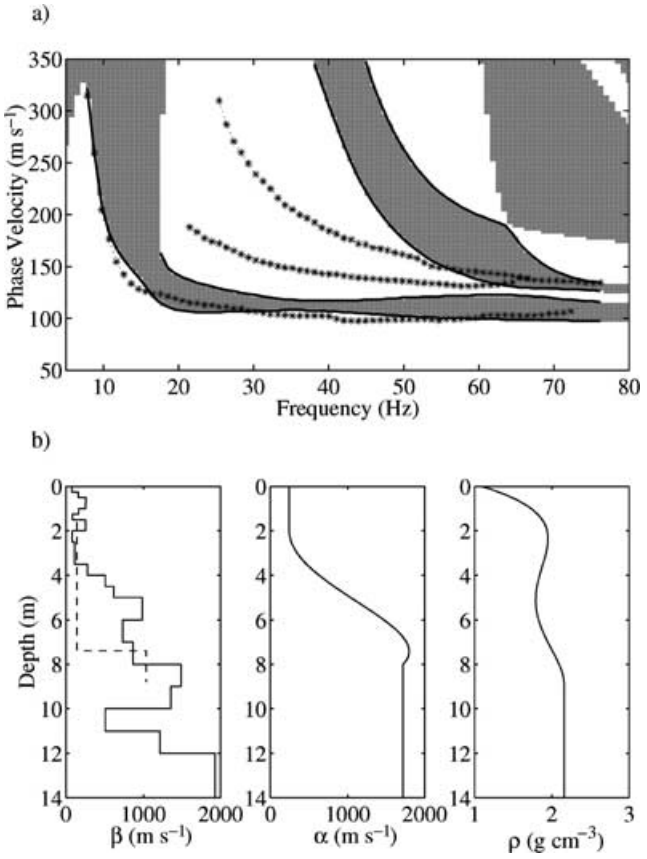

Figure 10. (a) Inversion results using 21 independent layers to represent the shear wave velocity profile but using only the fundamental mode dispersion curve in the inversion process. White and grey bands represent positive and negative values, respectively. The solid lines represent the roots of the dispersion function and the data are plotted as asterisks. All of the dispersion curves are included for comparison even though only the fundamental mode was used in the inversion. Note that although a reasonable fit to the fundamental mode is obtained, the higher-order dispersion curves shown do not fit the dispersion data at all. (b) The shear wave velocity profile (solid line) shown in the left-hand panel is the result of an inversion where 21 independent layers were used to represent the profile. Uncertainty analysis was not carried out in this case. The dashed line is the *S*-wave profile obtained from the VSP survey. The *P*-wave (middle) and density (right) profiles were held constant.

information. Resolution of the inverted velocity profiles is excellent (uncertainty <25 m s^{-1}) down to a depth of $\sim$7 m, after which the uncertainty increases to $\sim$500 m s^{-1} for a velocity of slightly less than 1000 m s^{-1}.

The inversions carried out using Chebyshev polynomials to represent the velocity profiles tend to run in shorter time and to be more stable than profiles represented by a set of discrete independent layers. The inversion in which the velocity of each of the layers has been allowed to vary independently, however, produces a smaller misfit overall. This suggests that the true velocity transition near 8 m depth is more rapid than that allowed by the Chebyshev profiles. This sharp change is consistent with the lithological boundary between the clay lacustrine deposits and the underlying stiff glacial tills.

Simulated annealing has proven to be quite useful for determining velocity profiles from dispersion curve data but is computationally quite expensive. There are several other methods of inversion that may be worthy of examination for future work in this area. The variational method (Takeuchi & Saito 1972; Aki & Richards 1980) offers a linearization of the problem that is more accurate than finding partial derivatives of the dispersion curve using numerical techniques (Novotný 1976). Perhaps a hedgehog-type method, as suggested by Kennett (1976) would provide the best compromise between linear and non-linear inversion techniques.*

Future areas of research that should be considered include designing a survey better able to examine attenuative properties, incorporating attenuation into the forward modelling and inversion algorithms, and expanding the knowledge base on near-surface properties with complimentary laboratory studies dealing with the effects of saturation state on materials. Also, the use of lower-frequency geophones would increase the depth of investigation, while a shear wave source could be used to improve the generation of Love waves that could be employed in conjunction with Rayleigh waves to improve the reliability of the inverted shear wave velocity profiles.

ACKNOWLEDGMENTS

This work is sponsored by NSERC and the Seismic Heavy Oil Consortium. Technicians L. Tober and M. Lazorek aided in data acquisition as did numerous graduate students. KSB acknowledges the support of an NSERC PGS-A scholarship.

REFERENCES

Abo-Zena, A., 1979. Dispersion function computations for unlimited frequency values, *Geophys. J. R. astr. Soc.,* **58,** 91–105.

Aki, K. & Richards, P.G., 1980. *Quantitative Seismology,* Freeman, New York.

Arfken, G.B. & Weber, H.J., 1995. *Mathematical Methods for Physicists,* 4th edn, Academic Press, New York.

Beaty, K.S., 2000. Determination of near-surface variability using Rayleigh waves, *Master's thesis,* University of Alberta, Edmonton.

Chunduru, R.K., Sen, M.K. & Stoffa, P.L., 1996. 2-D resistivity inversion using spline parameterization and simulated annealing, *Geophysics,* **61,** 151–161.

Efron, B. & Tibishirani, R., 1993. *An Introduction to the Bootstrap,* Chapman and Hall, London.

Ewing, W.M., Jardetzky, W.S. & Press, F., 1957. *Elastic Waves in Layered Media,* McGraw-Hill, New York.

Fowler, C.M.R., 1990. *The Solid Earth,* Cambridge University Press, Cambridge.

Ganji, V., Gucunski, N. & Nazarian, S., 1998. Automated inversion procedure for spectral analysis of surface waves, *J. Geotech. Geoenv. Eng.,* **124,** 757–770.

Geman, S. & Geman, D., 1984. Stochastic relaxation, Gibb's distribution and Bayesian restoration of images, *IEEE Trans.,* **PAMI-6,** 721–741.

Grechka, V.Y., McMechan, G.A. & Volovodenko, V.A., 1996. Solving 1-D inverse problems by Chebyshev polynomial expansion, *Geophysics,* **61,** 1758–1768.

Haskell, N.A., 1953. The dispersion of surface waves on multilayered media, *Bull. seism. Soc. Am.,* **43,** 17–24.

Ingber, L., 1989. Very fast simulated re-annealing, *Mathl. Comput. Model.,* **12,** 967–993.

Kausel, E. & Peek, R., 1982. Dynamic loads in the interior of a layered stratum: an explicit solution, *Bull. seism. Soc. Am.,* **72,** 1459–1481.

*For a hedgehog-type method a model is chosen through a Monte Carlo technique and then the area surrounding the model in parameter space is tested using the linearized formulation of the problem until the boundary of solutions that are compatible with the data is mapped out. A new area is chosen through Monte Carlo and the procedure is repeated.

Kausel, E. & Roesset, J.M., 1981. Stiffness matrices for layered soils, *Bull. seism. Soc. Am.,* **71,** 1743–1761.

Kennett, B.L.N., 1976. The inversion of surface wave data, *Pure appl. Geophys.,* **114,** 747–751.

Kirkpatrick, S., Gelatt, C.D. Jr & Vecchi, M.P., 1983. Optimization by simulated annealing, *Science,* **220,** 671–680.

Knopoff, L., 1964. A matrix method for elastic wave propagation, *Bull. seism. Soc. Am.,* **54,** 431–438.

Lay, T. & Wallace, T.C., 1995. *Modern Global Seismology,* Academic Press, New York.

Long, L., Chen, X., Doll, W., Kocaoglu, A. & Martin, J., 1999. Surface-wave group-velocity tomography applied to shallow structures at a waste site, in *Expanded Abstracts,* pp. 496–499, Society of Exploration and Geophysics.

Martinez, M.D., Lana, X., Olarte, J., Badal, J. & Canas, J.A., 2000. Inversion of Rayleigh wave phase and group velocities by simulated annealing, *Phys. Earth planet. Inter.,* **122,** 3–17.

McMechan, G.A. & Yedlin, M.J., 1981. Analysis of dispersive waves by wave-field transformation, *Geophysics,* **46,** 869–874.

Menke, W., 1979. Comment on 'Dispersion function computations for unlimited frequency values' by Anas Abo-Zena, *Geophys. J. R. astr. Soc.,* **59,** 315–323.

Metropolis, N., Rosenbluth, A., Rosenbluth, M., Teller, A. & Teller, E., 1953. Equation of state calculations by fast computing machines, *J. Chem. Phys.,* **21,** 1087–1092.

Miller, R., Xia, J., Park, C., Ivanov, J. & Williams, E., 1999a. Using MASW to map bedrock in Olathe, Kansas, in *Expanded Abstracts,* pp. 433–436, Society of Exploration and Geophysics.

Miller, R., Xia, J., Park, C., Moore, L. & Shefchik, W., 1999b. Seismic techniques to delineate dissolution features in the upper 1000 ft at a power plant site, in *Expanded Abstracts,* pp. 492–495, Society of Exploration and Geophysics.

Miller, R.D., Xia, J., Park, C.B. & Ivanov, J.M., 1999c. Multichannel analysis of surface waves to map bedrock, *Leading Edge,* **18,** 1392–1396.

Nazarian, S. & Stokoe, K.H., 1986. Use of surface waves in pavement evaluation, *Trans. Res. Rec.,* **1070,** 132–144.

Novotný, O., 1976. Methods of computing the partial derivatives of dispersion curves, *Pure appl. Geophys.,* **114,** 765–773.

Press, W.H., Teukolsky, S.A., Vetterling, W.T. & Flannery, B.P., 1997. *Numerical Recipes in C: the Art of Scientific Computing,* Cambridge University Press, Cambridge.

Rix, G.J. & Leipski, E.A., 1991. *Accuracy and Resolution of Surface Wave Inversion,* pp. 17–32, Am. Soc. Civ. Eng.

Roth, M. & Holliger, K., 1999. Inversion of source-generated noise in high-resolution seismic data, *Leading Edge,* **18,** 1402–1404, 1406.

Schwab, F.A., 1970. Surface-wave dispersion computations: Knopoff's method, *Bull. seism. Soc. Am.,* **60,** 1491–1520.

Schwab, F.A. & Knopoff, L., 1972. Fast surface wave and free mode computations, *Meth. Comput. Phys.,* **11,** 87–180.

Sen, M. & Stoffa, P.L., 1995. *Global Optimization Methods in Geophysical Inversion,* Elsevier, Amsterdam.

Stokoe, K.H. & Nazarian, S., 1985. *Use of Rayleigh Waves in Liquefaction Studies,* pp. 1–17, Am. Soc. Civ. Eng.

Stokoe, K.H., Wright, S.G., Bay, J.A. & Roësset, J.M., 1994. *Characterization of Geotechnical Sites by SASW,* pp. 15–26, Oxford Publishers, Oxford.

Szu, H. & Hartley, R., 1987. Fast simulated annealing, *Phys. Lett. A.,* **122,** 157–162.

Takeuchi, H. & Saito, M., 1972. Seismic surface waves, *Meth. Comput. Phys.,* **11,** 217–295.

Thomson, W.T., 1950. Transmission of elastic waves through a stratified solid medium, *J. Appl. Phys.,* **21,** 89–93.

Tokimatsu, K., Tamura, S. & Kojima, H., 1992. Effects of multiple modes on Rayleigh wave dispersion characteristics, *J. Geotech. Eng.,* **118,** 1529–1543.

Watson, T.H., 1970. A note on fast computation of Rayleigh wave dispersion in the multilayered elastic half-space, *Bull. seism. Soc. Am.,* **60,** 161–166.

Wiggins, R.A., 1976. A fast, new computational algorithm for free oscillations and surface waves, *Geophys. J. R. astr. Soc.,* **47,** 135–150.

Wolf, J.P., 1985. *Dynamic Soil-Structure Interaction,* Prentice-Hall, Englewood Cliffs, NJ.

Xia, J., Miller, R.D. & Park, C.B., 1999. Estimation of near-surface shear-wave velocity by inversion of Rayleigh waves, *Geophysics,* **64,** 691–700.

Xia, J., Miller, R. & Park, C.B., 2000. Advantages of calculating shear-wave velocity from surface waves with higher modes, in *Expanded Abstracts,* p. NSG 3.3, Society of Exploration and Geophysics.